The value of airborne wind energy to the electricity system

(article starts on next page)

RESEARCH ARTICLE

The value of airborne wind energy to the electricity system

Elena C. Malz[1] 🔘 | Viktor Walter[2] 🔘 | Lisa Göransson[2] 🔘 | Sebastien Gros[3] 🔘

[1]Electrical Engineering, Chalmers University of Technology, Gothenburg, Sweden

[2]Department of Space, Earth and Environment, Chalmers University of Technology, Göteborg, Sweden

[3]Department of Engineering Cybernetics, NTNU, Trondheim, Norway

Correspondence
Elena C. Malz, Electrical Engineering, Chalmers University of Technology, Gothenburg, Sweden.
Email: elenama@chalmers.se

Present address
Elena C. Malz, Department of Electrical Engineering, Signals and Systems, Chalmers University, 412 96 Göteborg, Sweden

Funding information
Chalmers Area of Advance

Abstract

Airborne wind energy (AWE) is a new power generation technology that harvests wind energy at high altitudes using tethered wings. The potentially higher energy yield, combined with expected lower costs compared to traditional wind turbines (WTs), motivates interest in further developing this technology. However, commercial systems are currently unavailable to provide more detailed information on costs and power generation. This study estimates the economic value of AWE in the future electricity system, and by that indicates which cost levels are required for AWE to be competitive. A specific focus is put on the relation between AWE systems (AWESs) and WTs. For this work, ERA-5 wind data are used to compute the power generation of the wind power technologies, which is implemented in a cost-minimizing electricity system model. By forcing a certain share of the annual electricity demand to be supplied by AWESs, the marginal system value (MSV) of AWE is investigated. The MSV is found to be affected by the AWE share, the wind resource, and the temporal distribution of the AWES's electricity generation. The MSV of AWE is location- and system-dependent and ranges between 1.4 and 2.2 $^{M\epsilon}/_{MW}$ at a low share of AWE supply (0%–30%). At higher shares, the MSV drops. The power generation of WTs and AWESs are related, implying that the wind technologies present a similar power source and can be used interchangeably. Thus, the introduction of AWESs will have a low impact on the cost-optimal wind power share in the electricity system, unless an AWES cost far below the system-specific MSV is attained.

KEYWORDS
airborne wind energy, electricity system modelling, marginal system value

1 | INTRODUCTION

Airborne wind energy (AWE) is an early-stage wind power technology investigated by industry and academia for the past decade. Airborne wind energy systems (AWESs) are tethered wings that harvest wind energy at high altitudes, which are inaccessible by conventional wind turbines. Since wind speeds are generally greater at higher altitudes, a higher energy yield for AWESs is expected. In addition, AWESs use less material than wind turbines (WTs), which is expected to result in lower costs.[1–3] However, these expectations and future prospects are based solely on estimations, since AWE is not yet commercially available, and it is uncertain how the technology will develop.[4] Industry is aiming for both small-scale off-grid solutions and large-scale (onshore and offshore) installations.[5–7] A roadmap of developing AWESs for large-scale usage is presented by Ampyx Power.[8]

The eventual large-scale deployment of a technology is highly dependent on its cost and its electricity generation relative to other technologies.[9] Large-scale deployment of AWE has been analysed based on reanalyses wind data resources,[10,11] and Lidar wind speed measurements have been evaluated at the location of Pritzwalk to estimate mid-altitude wind conditions and compute the optimal power production of an AWES.[12]

A common way to compare the economical potential of power generation technologies is the levelized cost of electricity (LCOE). As an example, in[13] the economic potential of an AWE park is evaluated using a quasi-steady flight model for the power curve estimation of the AWES. That work and most other studies[5,9,14,15] estimate that AWE technology could offer electricity at a lower LCOE compared to conventional wind turbines. The estimates of the LCOE for AWESs range between roughly 33 and 150 $^{M\epsilon}/_{Wh}$. The large span indicates that the actual costs are still highly uncertain. Apart from the LCOE, a crucial aspect of a power generation technology is the electricity generation profile, that is, the distribution of the electricity production in time. The work in Malz et al[16] computes the optimal power generation profile of AWESs and the one of traditional wind turbines, using MERRA-2 wind data from different locations. The power generation profiles of the two wind technologies are compared and found to be similar, especially at places with a low wind shear.[*]

So far, work has focused on assessing wind data for AWES operation, computing the power generation and assessing the economic potential of isolated AWESs. However, the role that AWE could play as a part of the electricity system has not been analysed in detail yet. Apart from the individual power production level of AWES units, their interaction with other power production technologies in the electricity system is of great importance. A generation profile that correlates with the net load of the electricity system has a high economical value. Here, the net load is defined by the system load minus renewable generation. In contrast, electricity generation that is concentrated to a few hours or that enhances the fluctuation of another electricity generation technology might be of less value to the system. Hence, the electricity generation profile of an AWES has a strong impact on its economic value in the electricity system.

The aim of this study is to investigate the economical value of the electricity generation from AWESs in four different regional electricity systems, accounting for the temporal distribution of the electricity. This study focuses on drag-mode AWESs. This type of AWESs generates the electric power by means of propellers on board and transfers it to ground via the tether.[2,17] In order to estimate the economical value of drag-mode AWESs, the annual generation profiles of two differently sized AWESs are modelled within four characteristic regions, with a temporal resolution of one hour and a spatial resolution of $0.25° \times 0.25°$. In Southern Sweden, this relates to an area of approximately 430 km[2]. Unlike the WT, which is modelled using a power curve for a 2 MW generator, the power generation of AWE is computed via a complex optimal control problem (OCP).[16,18,19] This approach accounts for physical limitations, for example, tether drag, and computes the maximal power production and optimal flight trajectory given prevailing wind speeds. The option of optimizing the flight trajectory and the operation height is an important advantage of AWESs compared to conventional WTs.[10]

The resulting computed electricity generation profiles are implemented in a regional cost-minimizing electricity system model that is formulated as a linear optimization problem.[20] The model is designed to investigate the interaction between different generation, load, and storage technologies and is built as a green-field model, that is, assuming no prior installed capacity. The technologies that are included in the model are coupled to their respective installation and power generation costs. In this study, instead of modelling the AWE technology related to an estimated cost, a certain installed AWE capacity is enforced in the electricity system model. The AWE generation profile is assumed to be a free source of energy. Hereby, the economical value of AWESs to the electricity system can be quantified in terms of the marginal system value (MSV). The MSV is the change in annual total electricity system cost divided by the change in installed capacity of AWESs. The computation of the MSV enables the estimation of the maximum cost of technology for being economical viable in a future emission-free electricity system. The MSV can be also interpreted as the 'willingness to pay' for adding AWE capacity to the system.

Since AWE technology is still under development, its value of AWE is mainly relevant for future electricity systems. This work therefore applies emission constraints and technology costs corresponding to 2050 projections.[21] The capacity installation and electricity production are optimized such that the demand is met at minimal costs and power plant constraints are fulfilled. This work is inspired by Göransson,[22] which uses a similar model to investigate the MSVs for different wind turbine designs. This work is also a follow-up study to Malz et al,[16] which presents a comparison between AWESs and WTs in terms of their generation profiles. Results of this work may indicate valuable directions for further AWE technology development and investments.

The article is structured as follows. Section 2 describes the wind data, the wind power generation technology models, and the electricity system optimization model and summarizes the studied scenarios. The results are presented in Section 3 and discussed in Section 4. Finally, Section 5 concludes the work.

2 | METHOD

This section describes the methods and data used for obtaining the in different regional electricity systems.

---

[*]A low wind shear means similar wind speeds at all relevant altitudes.

2.1 | Wind resource

In order to obtain accurate annual electricity generation profiles for both wind power technologies considered here, high-resolution wind data are needed. In this work, ERA-5 wind data from ECMWF[23] are used for all analysed regions. Wind data are acquired for the full year of 2012. The temporal resolution is hourly, and the horizontal spatial resolution of the data is 0.25° × 0.25°. The AWES model requires wind data at multiple altitudes in order to generate a vertical wind profile. The vertical wind data are given in 30 model levels (sigma levels), which are terrain-following pressure levels, that is, represent a specific geopotential above the surface.[24] The lowest level is about 10 m above surface and can vary from 1013 hPa at sea level to 500 hPa at 5 km in the Himalayas.[23]

From this wind data set, we consider the available altitude levels close to ground, such that we obtain 15 relevant vertical wind speed data points at each time and spatial instance. The wind speeds are given in their meteorological vector convention as u and v, corresponding to East/West and North/South wind speeds. The wind speed data are further processed into a family of smooth polynomial functions of the altitude. This interpolation is needed in order to estimate the wind speeds for the WT at the height of 100 m as well as to provide a vertical wind profile function to the AWES model. The procedure of transforming raw wind data to a polynomial function is explained in detail in previous work.[16,25]

2.2 | From wind power to electricity

For an accurate potential assessment of the two different wind power technologies, their power generation has to be computed with a WT model and an AWES model, respectively. In a large wind farm, the instantaneous wind speeds have local differences and are thus here assumed to be normally distributed over the farm. The standard deviation of the wind speed is dependent on the structure of the farm. In this study a standard deviation of $\sigma = 1^m/_s$ is assumed.[26] The affect on the wind farm power output can be seen in Figure 1. The higher the standard deviation the smoother is the cut-in and cut-out point of a wind farm.

2.2.1 | WT model

The power curve of a single turbine is formulated as

$$P_{WT,ind}(v_w) = \begin{cases} \eta_{ext} \min\left(\eta_{int} \frac{1}{2} c_p(v_w) \frac{\pi}{4} D^2 \rho v_w^3, P_{cap} \right) \frac{1}{P_{cap}} & \text{for } v_{in} \leq v_w \leq v_{out} \\ 0 & \text{otherwise,} \end{cases} \tag{1}$$

where the rotor diameter is $D = 100$ m and the generator size is $P_{cap} = 1.94$ MW, assuming the specific power of the wind turbine is 247 $^W/_{m^2}$. The internal and external losses are $\eta_{int} = 0.885$ and $\eta_{ext} = 0.94$, respectively. The efficiency c_p is a function of the wind speed v_w and varies
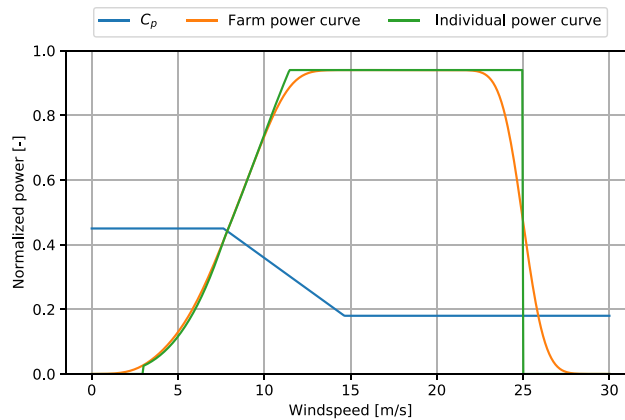

FIGURE 1 Power curve of an individual wind turbine and of a wind farm with a standard distribution of the wind speed of $\sigma = 1^m/_s$. The greater the standard distribution, the greater the smoothing effect. The power curve is limited to 94% to account for wind farm losses and maintenance downtime [Colour figure can be viewed at wileyonlinelibrary.com]

between 0.18 and 0.45.[22] The c_p-function can be found in Appendix A1. The cut-in and cut-out wind speeds v_{in} and v_{out} are assumed to be 3 and $25\,^m/_s$, respectively.

Compared to Equation (1), the power of a wind farm is assumed to be smoothed due to the normally distributed wind speeds in a farm. Here, a standard deviation of $\sigma = 1\,^m/_s$ is used.[26] The normalized instantaneous power produced by a farm is thus computed as

$$P_{WT,farm}(v_w) = \int_0^{30} f(x|v_w,\sigma^2) P_{WT,ind}(x)\, dx, \tag{2}$$

where f is the probability density function of the normal distribution. The standard deviation smooths the power generation curve at the cut-in and cut-out wind speeds. The effect for the wind turbine power curve is visualized in Figure 1.

The farm power density $\rho_{P,\,WT}$ of the WT farm is defined by the spacing of the wind turbines. In this study, the distance between the turbines is chosen to be seven times the rotor diameter, such that an area of $7D \times 7D$ is used for one turbine. This distance dependency is due wake and shadowing effects of neighbouring turbines. Given the specific power of the wind turbines of $247\,^W/_m$, this results in a farm power density of $3.95\,^{MW}/_{km}^2$.

2.2.2 | AWES model

For an AWES, the power generation of the AWES can not be defined by a machine power curve as the flight altitude is not constant, but varies for optimal power output. Thus, the AWES power is a function of the entire vertical wind profile and the optimal flight trajectory is dependent on the prevailing wind conditions. There exist different approaches of estimating the power production of an AWES, using static, quasi-steady or dynamic models of the AWES.[27-32] In this study, the model is formulated in the form of a dynamical system, and both the flight trajectory and the average power of the AWES are maximized for each wind profile. The system describes the AWE wing operating on a circular trajectory. The wing is modelled as a rigid body that is influenced by the prevailing wind speeds, the corresponding aerodynamic forces and control inputs. The method and the entire dynamical system is described in detail in previous studies.[18,33] As the power generation depends on the wind speeds at the current flight altitude, the dynamical system is implemented in an optimal control problem (OCP) that maximizes the average power generation of one flight orbit for a certain wind profile. This OCP is formulated as

$$\min_{\mathbf{x},z,\mathbf{u}} \quad \Phi(\mathbf{x},z,\mathbf{u},\mathbf{p},T) \tag{3a}$$

$$\text{s.t.} \quad F(\dot{\mathbf{x}},\mathbf{x},z,\mathbf{u},\mathbf{p},T) = 0, \tag{3b}$$

$$\mathbf{x}(0),\mathbf{x}(T) = 0, \tag{3c}$$

$$h(\mathbf{x},z,\mathbf{u},\mathbf{p},T) \leq 0, \tag{3d}$$

where the decision variables are the system states $\mathbf{x} \in \mathbb{R}^{22}$, the algebraic state $z \in \mathbb{R}^1$, and the control inputs $\mathbf{u} \in \mathbb{R}^4$. The system states $\mathbf{x}$ include position, velocity, rotation, angular velocity, surface controls and energy. The algebraic state z is connected to the algebraic tether constraint. The control inputs $\mathbf{u}$ include the change of surface controls and the drag force of the on-board propellers. The parameters $\mathbf{p}$ include the wind data. The cost functional $\Phi(\cdot)$ (3a) maximizes the average power generation of one trajectory during the orbit time T and regularizes the control inputs. The system function (3b) describes the flight dynamics, detailed in previous studies.[16,33] The constraints (3c) enforce periodicity of the flight trajectory, and (3d) introduces physical system bounds given by the physics of the AWES. A detailed description of the model and the OCP is given in a previous study.[19]

Since no commercial AWES is available yet, two possible systems are considered. The system configurations and parameters are aligned to the Makani wings,[34,35] which are described in more detail in previous studies.[16,19] The two drag-mode systems that are analysed are a large AWES (LAWES) with 2 MW (40 m wing span) and a small AWES (sAWES) with 0.6 MW (28 m wing span).

The OCP (3) is highly nonlinear and therefore challenging to solve. To generate an annual hourly electricity generation profile, the OCP needs to be solved repeatedly for the wind profile of each hour. A time-efficient numerical method of solving this large number of OCPs is proposed in a previous study.[25] That method exploits the similarity between consecutive OCP solutions resulting from different, yet similar, wind profiles. Furthermore, a regression model is trained and applied to approximate the mapping between the wind data and the power generation. Those methods are used to compute the power generation from all available wind data, taking into account the normal distribution of the wind speeds within a wind farm.

This procedure results in the normalized potential electricity generation profile of an AWE farm for each spatial grid point. The same procedure has also been used in the previous work of Malz et al,[16] in which the resulting power generation profiles, annual power production and capacity factor are listed in more detail.

The distance of the individual systems within a farm is assumed to be defined by the maximum tether length, which is here set to 500 m. The downwind direction of an AWES is determined by the current wind direction and thus the total space needed is in form of a dome with a radius of the tether length, measured from the ground station. This results in a AWE farm power density of $\rho_{P,sAWE} = 0.6$ and $\rho_{P,LAWE} = 2^{MW}/_{km}^2$, respectively. Related work minimizes the system spacing by assuming synchronous operation dependent on their optimal operation, and proposes a denser installation.[13,36,37] However, this study assumes conservative spacing, and includes a sensitivity analysis that takes different farm densities into account.

2.2.3 | Wind classes

The technology models and the available wind data thus yield an hourly electricity generation profile over one year for each spatial grid point and each modelled technology. The spatial resolution of this data relatively high ($0.25° \times 0.25°$) which results in a very large data set in the optimization problem. To reduce the number of data points and thus the model size, generation profiles are grouped into five wind classes. The simplification implies the assumption that wind power installations are geographically evenly distributed across each wind class and that there is no grid congestion within the investigated region. The five wind classes are defined by the percentiles of the average wind speeds at an altitude of 100 m. Each grid point is correspondingly assigned to a class dependent on its average wind speeds at 100 m, implying that each wind class collects a certain land surface area. The land surface area defined by a certain wind class for WTs is the same as that defined for that wind class for the AWESs. The wind speed interval and land surface area of the different classes can be found in Section 3 in Table 3 for each region, respectively. All generation profiles of a technology that fall within a certain wind class are averaged to one representative profile of that wind class. As a result, there are five wind classes per region, each comprising a location-independent available land surface area, as well as a representative generation profile for the WT, one for the sAWES, and one for the LAWES.

2.3 | Energy system model

The five AWE electricity generation profiles of all wind classes are implemented together with the five WT profiles into an electricity system model, formulated as a linear programming (LP) problem. It is formulated in GAMS and solved using the solver CPLEX.[38]

The model was originally developed in Göransson et al[39] as a regional investment and dispatch model to study thermal power plant cycling. The main decision variables of the LP problem are the regional installed capacity s of each technology and the hourly electricity generation g. The total electricity generation of all installed technologies must cover the hourly regional load at minimal annual system cost and net-zero CO_2 emissions. The model is set up as a green-field study, that is, assuming no prior installation of power plants. The purpose of the model is to study the dynamics of an eventual system with net-zero CO_2 emissions, rather than predicting the electricity system composition in the future. Thus, the green-field model is assumed to be a valid model choice. The modelled time resolution is three-hourly, perfect foresight is assumed, and distribution losses and ancillary services are neglected. The model thus captures the variability aspect of wind and solar power but neglects losses and the uncertainty aspect. Four model regions, Ireland (IE), Hungary (HU), south-central Sweden (SE2) and central Spain (ES3) are modelled, see more information in Section 2.5. Each region is modelled in isolation, that is, import and export of electricity are not considered. The main equations of the LP problem include the problem objective, that minimizes the annual system cost for investment and dispatch, as well as the constraining generation-load balance and the capacity limiting generation. This is mathematically defined as

$$\min c_{tot} = \sum_{i \in \mathcal{I}} AF_i C_i^{inv} s_i + \sum_{i \in \mathcal{I}} \sum_{t \in \mathcal{T}} (C_{i,t}^{run} g_{i,t} + c_{i,t}^{cycl}) \tag{4}$$

$$\sum_{i \in \mathcal{I}} g_{i,t} \geq D_t \quad \forall t \in \mathcal{T} \tag{5}$$

$$g_{i,t} \leq G_{i,t} \cdot s_i \quad \forall t \in \mathcal{T}, i \in \mathcal{I}, \tag{6}$$

where the decision variable c_{tot} is the total annual system cost. The variable s_i denotes the installed capacity of technology i, and $g_{i,t}$ the generation of technology i at time step t. Here, $\mathcal{I}$ denotes the set of included technologies and $\mathcal{T}$ the set of time steps (every third hour of the year). The parameter C_i^{inv} is the initial investment cost per technology and AF_i the annuity factor, which is dependent on the technical lifetime of a

TABLE 1 Technologies included in the model results

Technology	Description
AWE (1,2,3,4,5)	Airborne wind energy system of wind class 1,2,3,4,5 [1]
WT (1,2,3,4,5)	Onshore wind energy system of wind class 1,2,3,4,5
Hydro	Hydropower with storage
Nuclear	Nuclear power
PV	Photovoltaic with fixed optimal tilt (crystalline silicon cells)
CCBGT	Biogas-fuelled combined cycle gas turbine
BGT	Biogas-fuelled open cycle gas turbine
BNGCCS	Combined cycle gas turbine with CCS, fuelled by 90% natural gas + 10% biogas

Note: The land surface area that is defined by a wind class is the same for WTs and AWESs.

technology i and the interest rate of 5%. The parameter $C_{i,t}^{run}$ denotes the running costs, including variable O&M and fuel costs. The variable $c_{i,t}^{cycl}$ is the thermal cycling cost and the parameter D_t denotes the regional electricity demand at time t. The generation $g_{i,t}$ is limited by the installed capacity s_i and weighted by a parameter $G_{i,t}$, which is a weather-dependent profile for solar and wind power technologies. For the other technologies, $G_{i,t} = 1$ at all time steps t. All technologies in set $\mathcal{I}$ are listed in Table 1, and a list of included sets, variables and parameters can be found in Table B1. The technology data relevant for this study are listed in Table B2.

In order to include AWESs in the electricity system model and quantify their value to the system, relevant constraints and parameters have to be implemented in the electricity system model. One constraint affected by the inclusion of AWESs is the total land surface area per wind class available for wind power installations. With AWESs in place, the total land surface area available needs to be shared between AWESs and conventional wind turbines, which is formulated mathematically as

$$\frac{s_{WT\{k\}}}{\rho_{P,WT}} + \frac{s_{AWE\{k\}}}{\rho_{P,AWE}} = A_k \quad \forall k \in \{1,2,3,4,5\},\qquad(7)$$

where k is the wind class, $\rho_{P,\cdot}$ the power density $[^{GW}/_{km^2}]$ of AWE and WT, respectively, and A_k the available land surface area $[km^2]$ in class k. The land surface area related to the respective class is stated in Table 3. In this study it is assumed that AWESs and WTs cannot be placed at the same location. However, there are proposals of combining traditional wind turbines and AWESs.[29] The total area available in a region for wind power installations is reduced by inland waters, cities[40] as well as natural reserves NATURA2000[41] and other reserved land uses. This information is translated into a percentage specifying the available land surface area that is related to a spatial grid point.

Another important constraint is related to the calculation of the marginal system value (MSV). In this work, the total AWE power production (including curtailment), that is, the sum of all five wind classes, should supply a certain share ξ of the total regional electricity demand. This constraint is formulated as

$$\sum_{t \in \mathcal{T}} D_t \cdot \xi = \sum_{k=1}^{5} \sum_{t \in \mathcal{T}} s_{AWE\{k\}} G_{AWE\{k\},t},\qquad(8)$$

where $G_{AWE\{k\},t}$ is the regional generation profile of the AWE systems in class k.

In addition to the wind technologies, photovoltaic and hydro systems are part of the renewable power generation options available to the model. Various thermal generation fuelled by either solely biogas or biogas combined with natural gas with carbon capture and storage (CCS) and nuclear power generation are also included in the model. For the photovoltaic resource, an optimal-tilt device is modelled, using the formulation of Norwood et al[42] and the solar radiation data from MERRA in 2012.[43] Hydro power is only present in the region of SE2. The water inflow profile data is for 2012, taken from,[20] while the average inflow and regional distribution represents a typical hydrological year taken from Svensk Energi.[44] The costs of the thermal technologies and fuels are taken from the IEA World Energy Outlook 2016–2018[45] and from Thunman et al..[46] Costs of fuels and other technologies are found in a previous study.[47]

The remaining constraints and data that are related to technologies, resources, and emissions are given in the Appendix B1.

The methods and the data are taken from previous studies.[22,39] The model has been used for several studies focusing for example on electric vehicles[48] or traditional wind power.[22]

2.4 | Marginal system value (MSV)

In general, the electricity system model is an optimization problem designed to investigate the combination of electricity generation technologies that can meet the electricity demand at the lowest cost. The decision variables of the model include investments in electricity generation capacity as well as the three-hourly generation. Investment and running costs of different electricity generation technologies are key parameters in the model. As the costs of AWESs are still highly uncertain, the investment cost of the technology is not available.

Instead, the study uses the electricity system model in order to investigate the *marginal system value* (MSV) of AWESs. For this investigation, the available capacity of AWESs is fixed in the model such that it supplies a certain percentage of the annual electricity demand. The capacity installed of the other technologies are decision variables. The MSV denotes the change in electricity system cost with respect to an incremental change to the predefined fixed installed AWE capacity. Practically, the MSV is obtained by increasing the fixed AWE capacity step-wise between model runs, which results in less installed capacity by other technologies and thus changes in the investment and variable costs of the electricity system. As found in previous work,[22] the MSV varies greatly with the share of electricity that is supplied by the analysed technology; hence, the MSV is computed for different AWE shares.

To obtain the MSV for a specific AWE share ξ, that is, the share of the annual electricity demand that is supplied by AWE, first the *annual marginal system value* $c'(\xi)$ is obtained, mathematically described as

$$c'(\xi) = \frac{\Delta c_{\text{tot}}(\xi)}{\Delta s(\xi)} = \left| \frac{c_{\text{tot}}(\xi+0.05) - c_{\text{tot}}(\xi-0.05)}{s(\xi+0.05) - s(\xi-0.05)} \right| \quad \xi = 0, 0.1, ..., 1, \tag{9}$$

where $\Delta c_{\text{tot}}(\xi)$ is the change in total electricity system cost and $\Delta s(\xi)$ the change in installed AWE capacity at an AWE share ξ of the regional annual electricity demand. In this analysis, the share ξ is increased from 0 to 1 in discrete steps of 0.1. Note that, ideally, the total electricity demand equals the total generated electricity. This holds especially in this model as perfect foresight is assumed. Enforcing larger AWE shares as $\xi = 0.6 - 1$ entails AWE curtailment, as there is excessive supply at some hours of the year. Thus, even if the total annual AWE generation is fixed to be equal to the annual demand, there are other technologies needed in the electricity mix.

To obtain the value of $c'(\xi)$ from the model, the total AWE generation is constrained to a fixed share ξ of the regional annual demand. The cost for AWE power generation is set to zero, meaning AWE is a 'free' power source. Thus, the higher the share ξ, the higher the AWE capacity $s(\xi)$ and the lower the total system costs $c_{\text{tot}}(\xi)$. The change in costs Δc can then be related to the value of AWE in the system.

Looking at it from another perspective, $\Delta c_{\text{tot}}(\xi)$ is the 'willingness to pay' for the extra AWE capacity installed at a certain share ξ. To the readers it might be more informative to visualize the costs as projected initial investments, rather than annual costs. Thus, dividing the annual marginal system costs of Equation (9) by the annuity factor AF leads to the marginal system value $MSV(\xi)$ as

$$MSV(\xi) = c'(\xi) \cdot \frac{1}{AF} \quad \text{with} \quad AF = r^{-1}\left(1 - \frac{1}{(1+r)^t}\right), \tag{10}$$

where $r = 0.05$ is the interest rate and the expected AWE lifetime is $t = 30$.

The value of $MSV(\xi)$ corresponds to the upper bound of the combined investment and fixed O&M costs of a cost-competitive AWES.

2.5 | Studied scenarios

The study is performed for the four characteristic regions: (a) Ireland (IE), a windy region; (b) south-central Sweden (SE2), a windy and hydro-dominated region; (c) central Spain (ES3), a low wind but sunny region; and (d) Hungary (HU), a region with medium wind and solar radiation. These four representative regions are chosen to exemplify the impact of differences in renewable energy resources. An electrification of the industrial sector is assumed by 2050, which is estimated to increase the annual electricity demand by 22.5% compared to todays electricity demand levels given by ENTSO-E (2017).[49] The resulting electricity demand per region is listed in Table 2 and Table 3.

The available area and the total power density of AWE systems depend on several factors, such as the power density of a wind farm, the social acceptance of the technology, and the requirements on the installation site. These factors are assumed to be location independent, thus as the available installation area is not location dependent, all these factors can be reflected in the farm power density $[^{\text{MW}}/_{\text{km}}^2]$. Thus, the final power density is a product of the initial system density ρ_P and a density factor κ. This study uses two density factors $\kappa = \{0.1, 1\}$. For the wind turbine, a constant factor of 0.1 is used, which means that wind parks can be installed at 10% of the available land.[9,22] The scenarios that are modelled in each region are summarized in Table 2 and Table 3.

The marginal system value is then obtained by varying the share of the annual electricity demand supplied by AWESs in all these scenarios. This share ranges from 0 to 1.

TABLE 2 Electricity demand and land surface area available for wind power by region. Properties of the large AWES (LAWES), small AWES (sAWES), and WT: capacity, density, and the density factor κ.

Regions	Description	Demand [GWh]	Area [km²]
SE2, Sweden	Windy & hydro	92,491	145,076
ES3, Spain	Less windy & sunny	82,602	129,560
IE, Ireland	Windy & less sunny	29,332	50,646
HU, Hungary	Medium windy/sunny	40,334	65,992

TABLE 3 Properties of the large AWES (LAWES), small AWES (sAWES), and WT: capacity, density, and the density factor κ.

Technology	Size per unit [MW]	Farm power density [$^{MW}/^2_{km}$]	κ [−]
sAWES	0.6	0.6	{0.1, 1}
LAWES	2	2	{0.1, 1}
WT	2	3.96	{0.1}

To complement the MSV calculations, an additional approach to investigate the role of AWE in electricity systems is taken. Instead of the varying electricity share of AWE, a potential cost is assigned to the AWES technology, which is varied in different model runs. For a comprehensive comparison, the included AWES costs (investment and O&M costs) are set relative to the WT costs, ranging from 0.5 to 1.2. As a result, the relation between traditional wind turbines and AWESs can be investigated in more detail.

Note that in this analysis, the sAWES and the LAWES are implemented in individual model runs. This is done to separate the system dynamics to obtain a clear interpretation and because it is assumed that the technology development will converge to the AWE configuration that is most relevant in the future electricity system.

3 | RESULTS

This section presents the representative data within the wind classes and the analysis of the marginal system value (MSV) of AWE in the four different modelled regions. Table 4 lists land area and wind speed range at 100 m altitude for the different classes and regions. Clearly, the wind resources vary across regions, and wind speeds in class five in low-wind regions (HU, ES3) equal the wind speeds in low classes for the high-wind areas (SE2, IE)

Figure 2 shows the MSV for the four regions and four AWES cases, the sAWES and LAWES with $\kappa = 0.1$ and 1, respectively.

The horizontal grey dashed line represents a reference MSV of 1541 $^{k€}/_{MW}$, which equals the cost of the representative 2 MW wind turbine, consisting of the capital cost (1290 $^{k€}/_{MW}$) and the projected O&M cost for the given average full load hours (FLH) for 30 years of operation.

In the modelled cases, the MSV of AWE reaches up to $MSV(\xi = 0) = 2.2^{M€}/_{MW}$(SE2), which means that the AWES may cost 150% of the WT and still be valuable to the electricity system (Figure 2A at low AWE shares). MSV(0) is the extreme point of the MSV curve and describes the case of AWE entering the electricity system with its very first units. In general, the MSV of the AWESs varies between the regions, ranging at low electricity share levels from 1.3 to 2.2 $^{M€}/_{MW}$ and at high shares from 0.4 to 1 $^{M€}/_{MW}$. The corresponding LCOE can be estimated for the individual MSV levels and cases by multiplying the MSV with the annuity factor and dividing by the respective annual FLHs. As a result, a range of 35–45 $^{€}/_{MWh}$ is obtained for low share levels, representing the maximal cost-competitive LCOE in the modelled electricity system. This can be compared to the estimated range of 33 $^{€}/_{MWh}$ and 150 $^{€}/_{MWh}$, in previous studies.[5,9,14,15]

The explicit level of the MSV for the different modelled cases in Figure 2 is found to be determined by the following four factors:

(i) the AWE share of power generation;
(ii) the power density ($^{MW}/^2_{km}$) of the AWESs;
(iii) the AWE FLHs; and
(iv) the temporal distribution of the AWE power generation, that is, the profile value.

In the following, the four factors are discussed in detail.

3.1 | Impact of AWE share on the MSV

With an increasing share of AWE capacity in the electricity system, Figure 2 shows a general declining trend of the MSV in all regions, that is, the value of adding AWESs to the system decreases. The reason is three-fold: the gradual replacement of WTs by AWESs, the increased need for thermal peak generation to manage the generation-load balance, and/or the electricity system gradually becoming saturated with wind power, resulting in increased wind energy curtailment. The MSV trends can be explained in more detail as follows.

TABLE 4 Land area [km^2] and wind speed range [$^m/_s$] for each region and wind class, and wind speed average $\overline{w}$ and total area $\sum A$ for each region

| Wind class	SE2		IE		ES3		HU	
	Area	Wind speed	Area	Wind speed	Area	Wind speed	Area	Wind speed
1	29,500	(0, 5.56]	14,150	(0, 6.52]	13,740	(0, 3.91]	8530	(0, 4.55]
2	34,530	(5.56, 5.87]	14,640	(6.52, 6.69]	23,650	(3.91, 4.38]	11,370	(4.55, 4.83]
3	35,740	(5.87, 6.23]	13,100	(6.69, 7.08]	30,100	(4.38, 4.87]	15,300	(4.83, 5.10]
4	35,620	(6.23, 6.72]	7030	(7.08, 8.25]	31,200	(4.87, 5.20]	16,300	(5.10, 5.37]
5	9700	(6.23, inf]	1730	(8.25, inf]	30,890	(5.20, inf]	14,480	(5.37, inf]
	$\sum A$	$\overline{w}$	$\sum A$	$\overline{w}$	$\sum A$	$\overline{w}$	$\sum A$	$\overline{w}$
	14,5090	6.21	50,650	7.32	129,580	4.55	65,980	4.93
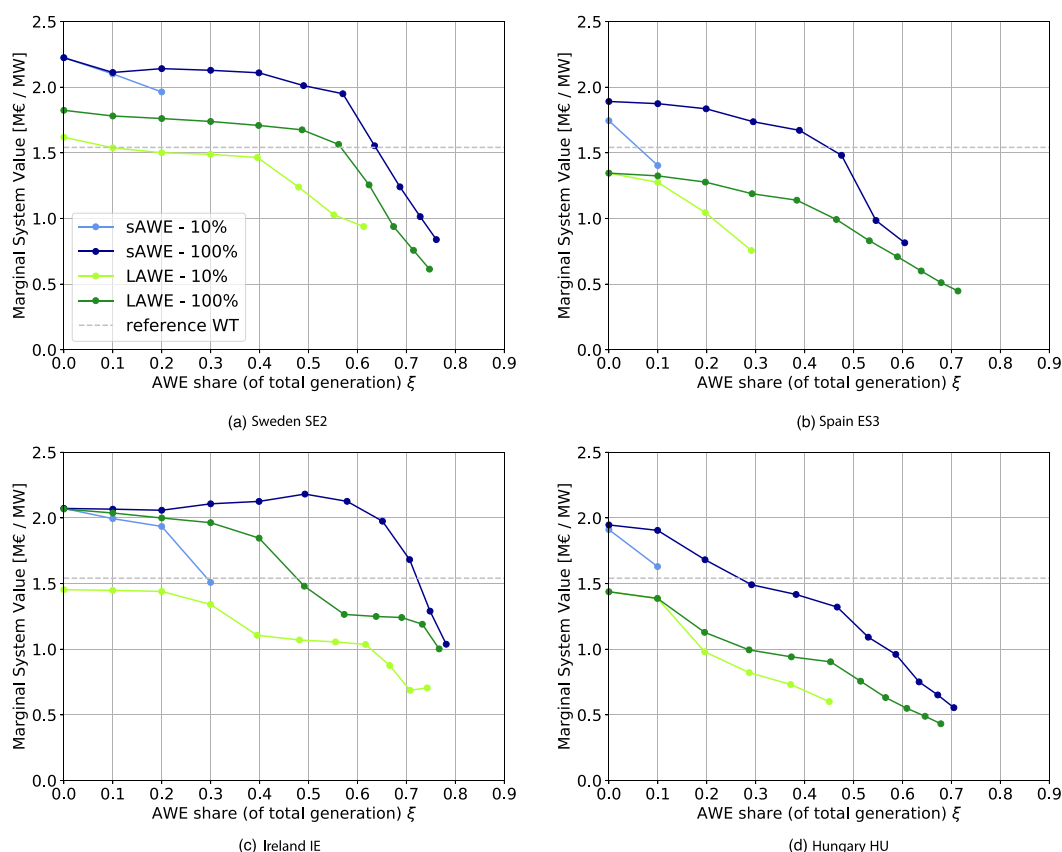
FIGURE 2 Marginal system value (*MSV*), corresponding to the system value of adding 1 MW AWE at different initial AWE shares (ξ) of the *total* produced annual electricity. The green lines show the large AWE system (LAWES) for the low density factor κ (10%) (light green) and high κ (100%) (dark green). The blue lines show the small AWE (sAWES) for the low (light blue) and high (dark blue) κ. The dashed grey horizontal line shows the projected capital and O&M cost of the reference wind turbine [Colour figure can be viewed at wileyonlinelibrary.com]
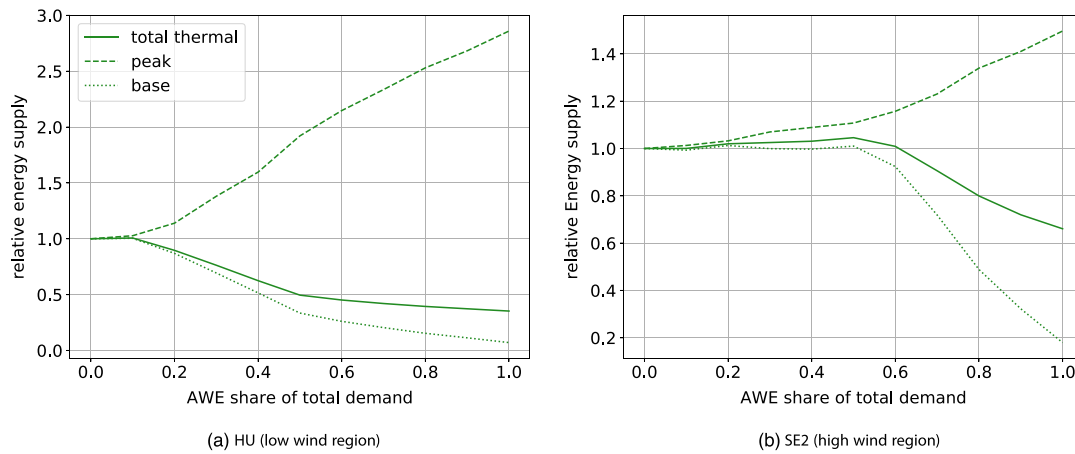
FIGURE 3 Thermal power generation as a function of AWE share relative to the zero-AWE case. Here, the LAWES-100% case is shown for regions HU (left) and SE2 (right). The peak generation (biogas GT and biogas CCGT) is plotted as a dashed line, the base generation (nuclear and bio+natural gas CCS) as a dotted line, and the total thermal production as a solid line [Colour figure can be viewed at wileyonlinelibrary.com]

At lower AWE shares, the MSV is almost flat for the windy areas of SE2 (for $\xi < 0.6$) and IE (for $\xi < 0.3$). This happens if within a 0.1-interval of ξ, AWESs repeatedly replace the WTs of one specific wind class, which implies that the total wind power generation in the system is more or less constant. With each ξ-step, the additional energy from AWE reduces the need for the same amount of WT capacity (Δs), accompanied by the same change in cost (Δc_{tot}), resulting in a constant MSV (see MSV definition, Equation 9).

The competition between wind technologies is discussed in more detail later.

At higher AWE shares, the system saturates, and the MSV declines more drastically. In other words, the technology 'outcompetes' itself. When the capacity of AWE is increased beyond a certain point, the total electricity generation fluctuates at such extent that wind power generation is curtailed. As a result, thermal base generation (in this study, mainly nuclear, and the bio+natural gas CCS) gets pushed out, and the hourly generation is then comprised by variable wind and solar power generation and costly thermal peak generation. The resulting declining MSV trend is clearly visible in Figure 2A beyond an AWE share of $\xi = 0.6$.

In order to visualize the relation between the wind power technologies and the thermal power generation in more detail, Figure 3 shows the thermal generation in the case of the LAWES for $\kappa = 100\%$ in regions SE2 and HU.

As can be seen, the greater the AWE share, the greater the thermal peak power generation (biogas GT and biogas CCGT), and the lesser the thermal base load technologies (nuclear and bio+natural gas CCS). In general, this indicates an increasing variability of the power supply in the electricity system. The electricity supply by peak power generation is costly, which causes the decline in MSV of AWE.

A more detailed investigation shows that during the gradual replacement of WTs by AWESs at low shares (see SE2 at $\xi < 0.6$ in Figure 3B), the peak power generation increases only slightly. This indicates the constant electricity share by wind energy, but also the higher generation variability of AWESs compared to WTs. Beyond that point of $\xi = 0.6$, the electricity system gets more and more saturated by general wind energy, entailing a more significant decline in thermal base production and incline in thermal peak production. As a result, the total thermal power generation drops, which is as expected due to the increased energy supply by wind power technologies and the resulting system saturation. In less windy regions like HU, the drop of all thermal production technologies and the wind energy saturation occurs at lower AWE shares, as the wind resource is low.

For the other modelled regions, the thermal power generation trends show slight differences but the general trend is similar for all, and hence the same conclusion is drawn for all regions.

There are rare cases of an increase in the MSV (Figure 2C, sAWE-100%). This happens if, at low shares, AWE capacity is installed in the low wind-speed classes, while, at higher shares, capacity shifts to high wind-speed classes. The same amount of energy can now be generated with less installed capacity, because installations in high-wind classes show a greater number of FLHs.[†] The relation between wind classes and FLHs is detailed in the next paragraph.

[†]This increasing effect is mainly due to the wind classes, which are a modelling choice made in this paper.

3.2 | Impact of number of FLHs, power density and profile value

The number of FLHs per class for each region and technology are shown in Figure 4.

The sAWES has many more FLHs than the LAWES, which is due to the greater area-to-weight ratio of the power-producing wing. This greater number of FLHs is closely linked to the greater MSV compared to the LAWES in Figure 2 (blue curves vs. green curves). Another cause for the better MSVs is the better profile value of the sAWES compared to the LAWES, that is, a more equally distributed power during the year with fewer zero production hours. A more constant power profile requires less costly thermal peak power generation, improving the system value. This difference in profile value impacts the final energy mix. As an example, in the SE2 region, the electricity production by thermal technologies is up to 13% higher for the LAWES compared to the sAWES case. This is visualized in Figure 5, that shows the electricity production by the thermal power plants in SE2.

The same trend can be observed for the other modelled regions as well. The higher profile value for the sAWE is also identified in a previous study.[16] However, the power density of the sAWES is three times lower. (In this study, $\rho_{sAWE} = 0.6\,^{MW}/_{km}^2 < 2\,^{MW}/_{km}^2 = \rho_{LAWE}$). The power density is relevant if the local area restriction becomes a limiting factor. The cases sAWE-10% and LAWE-10% cannot reach the high electricity shares due to lack of installation sites, visible in the limited 'shorter' MSV trends in Figure 2.

3.3 | Total wind energy share and wind class allocation

The same four key factors, i–iv, impact the competition between AWE and traditional WTs and determine the cost-optimal allocation of the technologies among the wind classes within a region. The general trend shows that it is cost-optimal to allocate AWE capacity to the lowest wind-speed classes that have WTs installed and to replace WTs in that class. In windy regions (SE2 and IE), that means classes 2–4. In poor wind regions (HU and ES3), WTs are only installed in class 5, where AWESs are thus also allocated.

This way of allocating AWESs and traditional WTs to the available sites takes advantage of the partly higher FLHs of AWESs relative to WTs (Figure 4) and leaves the high wind-speed sites to the WTs, as WTs show a more uniform power generation. The results also show that (at least in
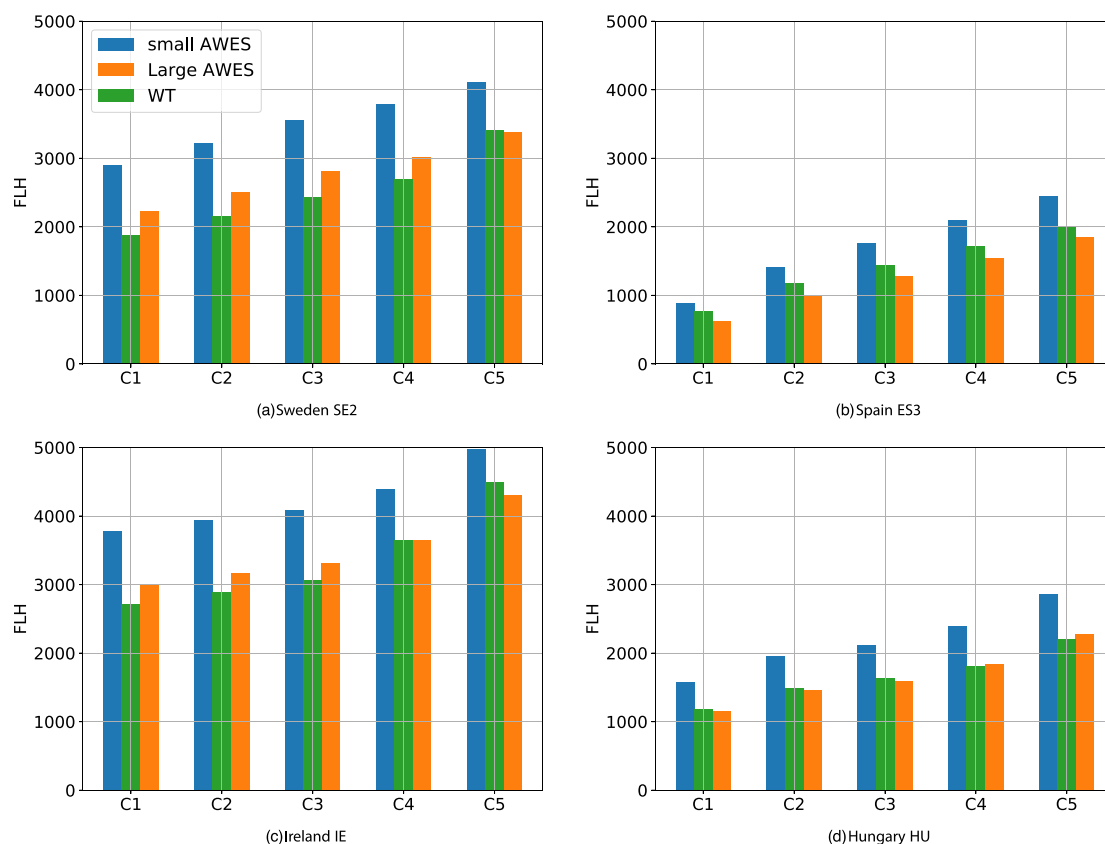

FIGURE 4 FLHs per each class for each region and technology. SE2 and IE are windier and result into more FLHs, while HU and ES3 are less windy with fewer FLHs. The small AWES has the highest FLHs for all cases [Colour figure can be viewed at wileyonlinelibrary.com]
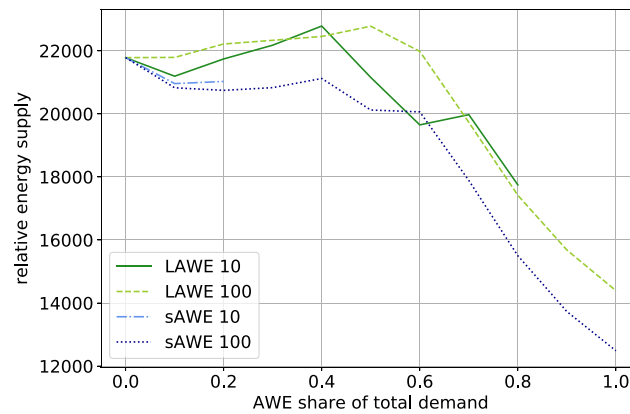
FIGURE 5 Thermal generation in the region of SE2 (Sweden) for all AWES cases. The trend shows that at almost all levels of AWE share, the thermal generation for the large AWE system is greater than for the small AWE system. This indicates that the generation profile of the large system is more variable than the profile of the small system [Colour figure can be viewed at wileyonlinelibrary.com]

SE2 and IE) the difference in profile value between high and low wind classes is greater for WTs than for AWE. Thus, it is more cost-efficient to place AWESs in the low-wind classes.

Figure 4B,D shows that in the less windy regions, the large AWES always has fewer FLHs than the WTs. Together with the low profile value, the resulting MSV of LAWESs is always below the reference cost of WTs (Figure 2B,D).

In order to visualize the wind technology allocations, the results of varying the AWE costs in the model are shown for some illustrative scenarios in Figure 6. In the figures, the electricity production mix is displayed for a range of relative AWE system costs [0.5, 1.2].

Figure 6A,B shows the optimal mix of the electricity production for the region SE2 in Sweden, meeting the annual electrical energy demand of 92,491 GWh. The surplus wind and solar production that is curtailed is not displayed. The optimal electricity mix consists of approximately 50% wind power, 13% hydro power, and 37% thermal power generation.

For clarification, these plots can be linked to the MSV results in Figure 2. The optimal energy mix for the case of equal costs for AWESs and WTs (relative cost AWE/WT = 1) in Figure 6A yields an AWE share of the electricity mix of ∼ 0.1. Considering an AWE share of 0.1 in Figure 2A, one can observe that the MSV of AWE equals the costs of WTs. Thus, one can find the same results in both figures, illustrating different perspectives and resolutions.

The result of this analysis highlights and confirms the two findings presented in the previous section. Firstly, AWE has to be much cheaper relative to WT in order to increase the total wind energy share. Secondly, AWE systems are preferentially allocated to the low wind-speed sites, while the WTs take the high wind-speed sites.

The first finding can be observed from the total share of wind energy in each modelled scenario. Unless the AWES is much cheaper or achieves a high power density, the total share of ∼50% wind power generation in SE2 is constant for all scenarios. Figure 6A shows that AWE becomes economical as soon as its cost matches the costs of traditional WTs (rel.cost = 1). If both technologies are part of the electricity production one technology replaces the other. This implies that the total share of wind power in the system does not change, even if AWE becomes economically viable. In fact, in the vast majority of the investigated cases, the AWESs simply replace traditional wind turbines as the cost of the AWES is reduced. This competition between the two technologies is explained by their very similar electricity generation profiles. Figure 6B presents the energy mix with the sAWES. The difference to the LAWES case is that due to its large number of FLHs, its installation is economical, even if it becomes more costly than traditional wind. However, also in this case, the total share of 50% wind power is not exceeded; traditional wind in in class 4 is simply replaced by AWE capacity.

The second finding concerning the allocation of the wind power technologies into the different wind classes is also observable in Figure 6. If WTs and AWESs are both part of the system, WTs take the high wind-speed areas while AWE systems take the low wind-speed areas. Only for the exception of very low AWE costs, for example, in Figure 6A, AWE is present in wind class 5. However, this class-5 area is assigned to traditional WTs if they are part of the total electricity production. Figure 6B suggests that a share of AWE is useful at all modelled cost levels, but in all cases the high wind-speed sites are equipped with WTs only.

As a last illustration, the FLHs of the different technologies are mapped over the SE2 region in Figure 7.

Note that a high number of FLH does not necessarily imply a good performance at low wind speed. The FLHs might be obtained by production concentrated on the medium and high wind speed hours. Coastal sites and Lake Vänern at location N59'E13' present equally good sites for all systems, that is, the FLHs are similar, and partly better for the WT (Figure 7A) than for the big AWE system (Figure 7C). These areas would relate to wind class five and thus present installation sites to WTs. On the other hand, the sites in the North show few FLHs for the WTs (the blue area), while the AWESs can claim higher FLHs. These areas would correspond to lower wind classes and be assigned to AWESs. For a
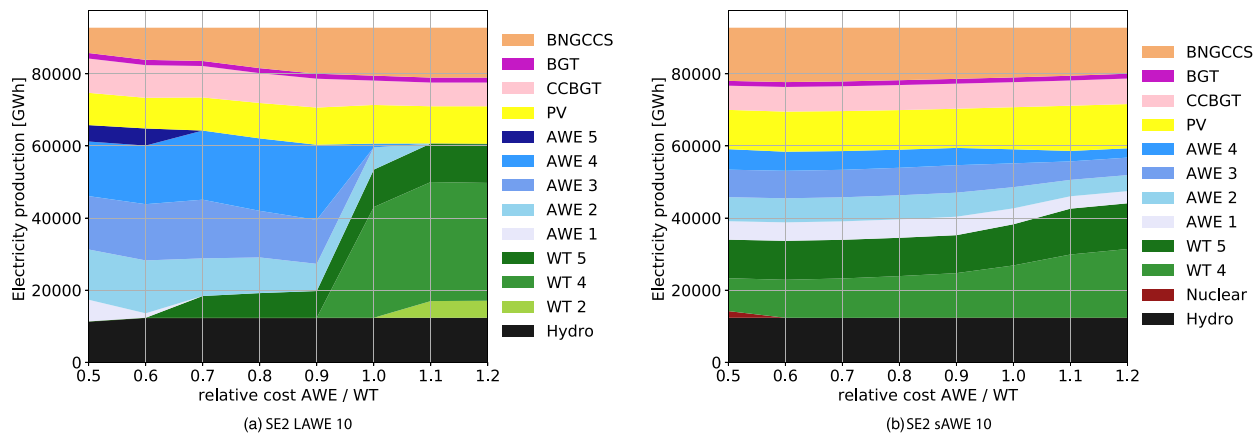
FIGURE 6 Optimal modelled annual energy mix for SE2, density factor $\kappa = 10\%$ for the LAWES (left) and the sAWES (right). The system is optimised with different investment and O&M for AWE. The cost (x-axis) is illustrated as relative cost compared to the modelled WT cost. The results demonstrate how the class areas are allocated among the wind power technologies and how the technologies are competing. The included technologies are described in Table 1 [Colour figure can be viewed at wileyonlinelibrary.com]
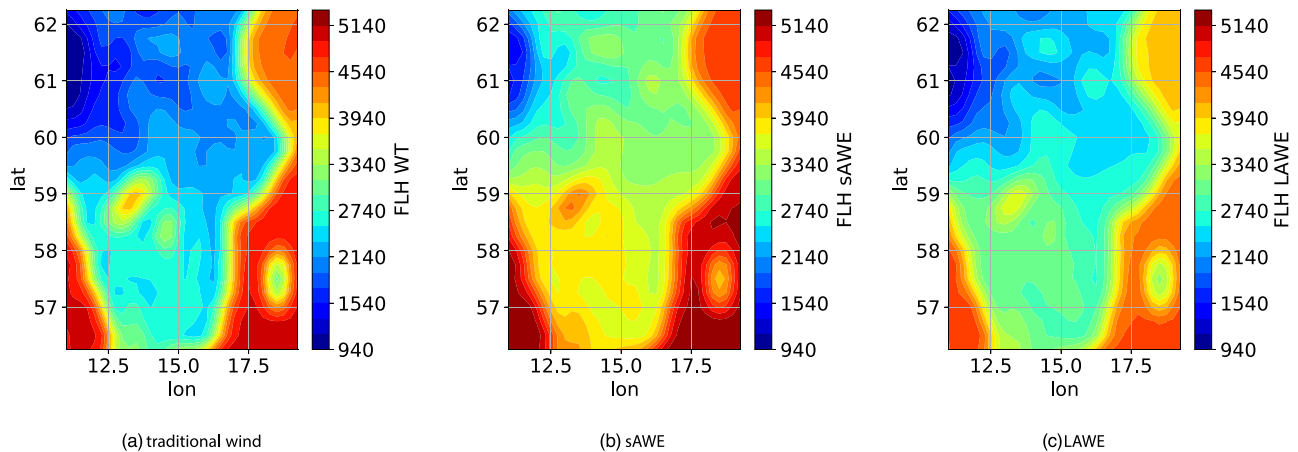

FIGURE 7 Map of SE2, showing the average FLHs for each technology, WT, sAWES, and LAWES. The WT shows the lowest FLHs in the Northern part, which makes those areas more attractive for AWESs. Coastal areas are similar for all wind power technologies, making the power density the main decision factor for the technology allocation. These figures show the resource potential and are independent of the assumed power density [Colour figure can be viewed at wileyonlinelibrary.com]

more thorough visualization, the difference between the number of FLHs from the AWESs compared to those from the WT is displayed in Figure 8.

The plots show the regions in which the modelled AWESs would have an advantage in FLHs compared to the WT. The figure indicates that the inland and hilly areas give AWESs over WTs a greater advantage than coastal and offshore areas. Similar findings have been presented in an earlier study,[16] where the computed power production of the AWESs and WT are compared at specific location points. In that study one important finding is the importance of the wind shear for the performance of AWESs. The greater the wind shear the greater is the advantage for AWESs to make use of the high-altitude winds and the option of an adjustable operation altitude. At locations with similar wind speeds at all altitudes a low operation altitude is sufficient and WTs, that have a lower cut-in wind speed, show a comparable better power yield. An investigation of the temporal average wind shears of the studied regions is beyond the scope of this work.

The remaining modelled scenarios result in the same findings and are therefore not shown here.

4 | DISCUSSION

This section discusses the consequences of assumptions, limitations and model choices.

(a) Difference in FLH of sAWE compared to WT   (b) Difference in FLH of LAWE compared to WT
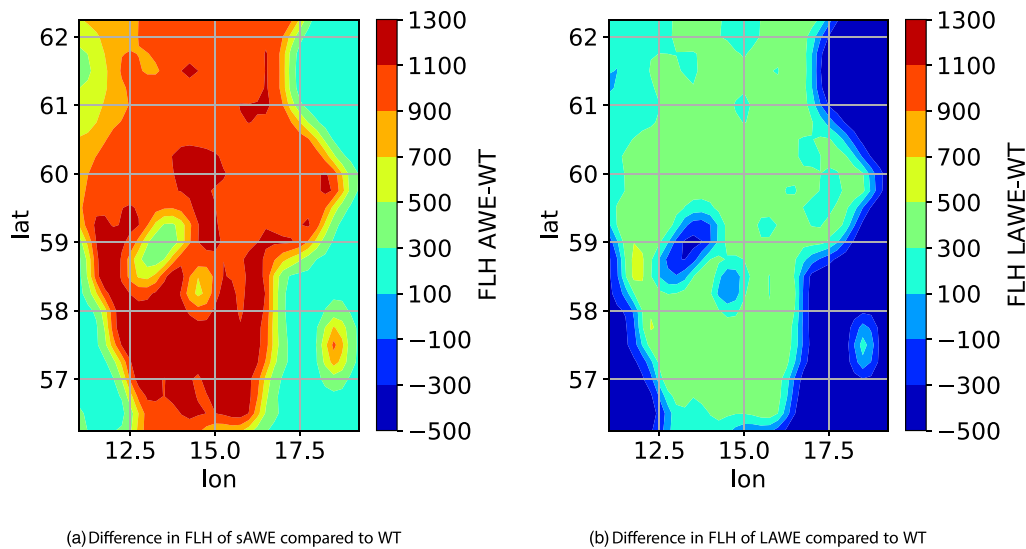
FIGURE 8 Difference in absolute FLHs of the AWESs compared to WT in the case of SE2. As can be seen, the sAWES shows an advantage compared to the LAWE [Colour figure can be viewed at wileyonlinelibrary.com]

The power generation of the wind power systems as well as the optimization of the electricity grid are modelled assuming perfect foresight on weather and demand. This assumption mainly affects the cases using intensive thermal base load. Excluding the weather uncertainty, the costs of wind integration are underestimated as thermal power cycling is planned with perfect information available.

There are two uncertain density factors relevant to the results of this work: the available space and the AWE farm density. Available space is dependent of land and airspace regularisation as well as acceptance.[9] AWE farm density depends on the choice of a safety margin, ranging from one system to multiple systems per km^2.[36,37] Due to this uncertainty, here AWE density is varied by introducing a location-independent density factor κ and the locations are modelled for two different values, $\kappa = 10\%$ and 100%. A complete space availability is unlikely, but a higher farm density can be obtained by sophisticated control of the system. A higher space availability or a higher farm density can be related to the $\kappa = 100\%$ case. An explicit density case cannot be extracted from the modelling, but the two density factors cover a theoretical span between low farm density and low area availability to high farm density and higher area availability.

In this study, the electricity system is modelled without storage technologies, such as batteries, fuel cells, or fly wheels. With the expected reduction in battery costs and the introduction of electrical vehicles, energy storage is an important and influencing factor in the future electricity system.[21] Also, demand side management (DSM) is disregarded in the modelled scenarios. However, the profile values of AWESs and WTs are both affected by these assumptions, and it is questionable if there would be an impact on the relation between the two technologies.

The electricity system is modelled for isolated regions, not allowing trading in any way. This is an unrealistic case and, like the lack of the storage devices, it dismisses the possibility of smoothing variable power generation and demand. However, electricity trading would blur the regional system dynamics, making the interaction between different electricity generation technologies less apparent.

The results indicate quite a difference between the small and the large AWES. The modelling results for the sAWES of 666 kW show a power profile of higher value and more FLHs than the LAWES. This is explained by the lower weight per wing area and the lower tether drag, stemming from a thinner power cable. A similar conclusion has been drawn for the sAWES in a previous study.[16] However, considering the required land area, it is questionable whether the system with the lower power density per system is targeted for large-scale deployment.[9] This will largely depend on the density at which the wind farm can be operated. The LAWES has a lower MSV than the sAWE (up to 30%) and is in most cases less valued than a WT (up to 10%), as seen in Figure 2.

For most modelled scenarios, the optimal allocation of the AWESs has been in the lowest wind-speed classes in which WTs are initially installed, which can be a decisive factor in the planning and placement of funding. The factors that should be sought to be maximized are the farm power density, FLHs, and acceptance. Note that offshore locations are not taken into account in this study. AWE investors are looking into deep offshore solutions and considering AWE based on a floating foundation.[6,7] Including these possibilities might enhance the AWE value and could increase the total wind power share in the electricity mix. Also, storage and load balancing within an AWE farm could compensate for their less even generation profile and hereby enhance the value of their generation. However, this comes with an increased cost.

The AWE power profiles are obtained by optimizing a drag-mode system. It is uncertain how the results differ for pumping-mode systems. Lloyd predicted in a previous study[50] that the total power generation is similar for both systems, which would result in similar conclusions for both AWESs. However, the instantaneous power generation might vary. The comparison is beyond the focus of this paper and is left for future investigations.

5 | CONCLUSIONS

This work investigates the economic value of airborne wind energy systems (AWESs) in a conceptional future electricity system in terms of their marginal system value (MSV). The modelled scenarios consist of four drag-mode AWES cases, a large wing with a capacity of 2 MW and a small wing with 0.6 MW, and with a high and a low power density factor per land area for each. The electricity generation profiles of the AWESs are obtained by optimizing the flight trajectory of the AWES, taking into account the hourly wind conditions at various altitudes. The value of the AWE systems is investigated for four regions, which differ in conditions for renewable electricity generation and seasonal distribution of the electricity demand. From the results it can be concluded that:

- The marginal system value of AWESs varies for low electricity shares between 1.3 and 2.2 $^{M\epsilon}/_{MW}$. The corresponding LCOE range is $35-45\frac{\epsilon}{MWh}$, which corresponds to the lower bound of the AWE costs estimated by previous work. At high shares, the MSV lies between 0.4 and 1 $^{M\epsilon}/MW$.
- The total share of wind energy in the electricity system is not increased by introducing AWESs. This is due to the WT and AWES power profiles being very similar, so that the other technology is simply replaced, dependent on the system cost and an eventual system saturation.
- In regions with generally good wind conditions, the value of AWE is highest when replacing traditional WTs on poor wind sites, while the high-wind sites are left for traditional WTs. This is because AWESs have a higher number of FLHs, but a less even generation profile compared to WTs. In less windy regions like HU and ES3, there is generally little wind resource available, so that wind power is mainly only installed in the highest wind class.
- The main factors that should be pursued for a high system value are a high system power density, a high number of FLHs (relative to for WTs), and low variability in the generation profile during the year. These factors positively affect the MSV of AWESs and thus promote the eventual commercialization of the technology.

In future work, the interplay of AWE and the electricity system should also be investigated for other AWES technologies as the pumping-mode system or the multi-kite AWES. Dependent on their generation profiles, their value to the electricity system might differ to drag-mode AWES. In addition, the work should be extended by including offshore areas. For a more thorough analysis, the heating and transport sector as well as storage technologies should be considered in the electricity system model. These aspects change the dynamics in the system and might have an impact on the economical value of AWESs.

ORCID
Elena C. Malz https://orcid.org/0000-0002-3541-5594
Viktor Walter https://orcid.org/0000-0003-1220-4441
Lisa Göransson https://orcid.org/0000-0001-6659-2342
Sebastien Gros https://orcid.org/0000-0001-6054-2133

REFERENCES
1. Zillmann U, Bechtle P. Emergence and economic dimension of airborne wind energy. In: Schmehl R, ed. *Airborne Wind Energy: Advances in Technology Development and Research*. Springer; 2018:1-25 10.1007/978-981-10-1947-0_1.
2. Cherubini A, Papini A, Vertechy R, Fontana M. Airborne wind energy systems: a review of the technologies. *Renew Sustain Energy Rev*. 2015;51: 1461-1476. https://doi.org/10.1016/j.rser.2015.07.053
3. U. Zillmann and S. Hach, "Financing strategies for airborne wind energy," in *Airborne Wind Energy*, U. Ahrens, M. Diehl, and R. Schmehl, Eds. Springer, 2014, pp. 117–137, doi: 10.1007/978-3-642-39965-7_7.
4. Watson S, Moro A, Reis V, et al. Future emerging technologies in the wind power sector: a European perspective. *Renew Sustain Energy Rev*. 2019; 113:109270. https://doi.org/10.1016/j.rser.2019.109270

5. Enerkite. Available at https://www.enerkite.de. (Accessed on: June 10, 2020).

6. Ampyx Power. Available at https://www.ampyxpower.com. (Accessed on June 19, 2020).

7. de Vries E., Floating offshore takes to the skies, Available at https://www.windpowermonthly.com/article/1466082/floating-offshore-take s-skies, May 2018.

8. Kruijff M, Ruiterkamp R. A roadmap towards airborne wind energy in the utility sector. In: Schmehl R, ed. *Airborne Wind Energy: Advances in Technology Development and Research*. Springer; 2018:391-411 10.1007/978-981-10-1947-0_26.

9. European Commission. Study on challenges in the commercialisation of airborne wind energy systems. Publications Office of the European Union, Tech. Rep., September 2018, doi: https://doi.org/10.2777/87591

10. Bechtle P, Schelbergen M, Schmehl R, Zillermann U, Watson S. Airborne wind energy resource analysis. *Renew Energy*. 2019;141:1103-1116. https://doi.org/10.1016/j.renene.2019.03.118

11. Archer CL, Delle Monache L, Rife D. Airborne wind energy: optimal locations and variability. *Renew Energy*. 2014;64:180-186. https://doi.org/10.1016/j.renene.2013.10.044

12. Sommerfeld M, Crawford C, Monahan A, Bastigkeit I. Lidar-based characterization of mid-altitude wind conditions for airborne wind energy systems. *Wiley Wind Energy*. 2019;22(8):1101-1120. https://doi.org/10.1002/we.2343

13. Faggiani P, Schmehl R. Design and economics of a pumping kite wind park. In: Schmehl R, ed. *Airborne Wind Energy: Advances in Technology Development and Research*. Springer; 2018:391-411 10.1007/978-981-10-1947-0_16.

14. Kitepower. Kitepower - airborne wind energy. Available at https://kitepower.nl. (Accessed on: June 10, 2020).

15. Mann S. An introduction to airborne wind technology and cost reduction trends. 2019.

16. Malz E, Hedenus F, Göransson L, Verendel V, Gros S. Drag-mode airborne wind energy vs. wind turbines: an analysis of power production, variability and geography. *Energy*. 2020;193:116765. https://doi.org/10.1016/j.energy.2019.116765

17. Diehl M. Airborne wind energy: basic concepts and physical foundations. In: Ahrens U, Diehl M, Schmehl R, eds. *Airborne Wind Energy*. Springer; 2013: 3-22.

18. Horn G, Gros S, Diehl M. Numerical trajectory optimization for airborne wind energy systems described by high fidelity aircraft models. In: Ahrens U, Diehl M, Schmehl R, eds. *Airborne Wind Energy*. Berlin, Heidelberg: Springer; 2013:205-218 10.1007/978-3-642-39965-7_11.

19. Malz EC Airborne wind energy—to fly or not to fly. Ph.D. dissertation, Chalmers University of Technology, 2020. [Online]. Available: https://research.chalmers.se/publication/518841/file/518841_Fulltext.pdf

20. Göransson L The impact of wind power variability on the least-cost dispatch of units in the electricity generation system. Ph.D. dissertation, Chalmers University of Technology, Available at: https://research.chalmers.se/en/publication/196126, 2014.

21. Jenkins J, Luke M, Thernstrom S. Getting to zero carbon emissions in the electric power sector. *Joule*. 2018;2(12):2487-2510. https://doi.org/10.1016/j.joule.2018.11.018

22. Johansson V, Thorson L, Goop J, et al. Value of wind power—implications from specific power. *Energy*. 2017;121:352-360. https://doi.org/10.1016/j.energy.2017.03.038

23. ECMWF. Copernicus Climate Change Service (C3S): ERA5: Fifth generation of ECMWF atmospheric reanalyses of the global climate, (2017).

24. ECMWF Model Levels. (Accessed on: November 10, 2020). [Online]. Available at: https://artefacts.ceda.ac.uk/badc_datadocs/ecmwf-op/levels.html

25. Malz E, Verendel V, Gros S. Computing the power profiles for an airborne wind energy system based on large-scale wind data. *Renew Energy*. 2020; 162:766-778. https://doi.org/10.1016/j.renene.2020.06.056

26. Olauson J, Bergkvist M. Modelling the Swedish wind power production using MERRA reanalysis data. *Renew Energy*. 2014;76:717-725. https://doi.org/10.1016/j.renene.2014.11.085

27. Machado JPR Estimation of energy production in aerial systems of Wind Energy, Msc Thesis, University of Porto, 2019, doi: https://hdl.handle.net/10216/121229

28. Ranneberg M, Wölfle D, Bormann A, Rohde P, Breipohl F, Bastigkeit I. Fast power curve and yield estimation of pumping airborne wind energy systems. In: Schmehl R, ed. *Airborne Wind Energy: Advances in Technology Development and Research*. Springer; 2018:623-641.

29. Lellis MD, Mendonça A, Saraiva R, Trofino A, Lezana A. Electric power generation in wind farms with pumping kites: an economical analysis. *Renew Energy*. 2016;86:163-172. https://doi.org/10.1016/j.renene.2015.08.002

30. Fechner U, van der Vlugt R, Schreuder E, Schmehl R. Dynamic model of a pumping kite power system. *Renew Energy*. 2015;83:705-716.

31. Licitra G, Koenemann J, Bürger A, Williams P, Ruiterkamp R, Diehl M. Performance assessment of a rigid wing airborne wind energy pumping system. *Energy*. 2019;173:569-585. https://doi.org/10.1016/j.energy.2019.02.064

32. Bauer F, Kennel RM, Hackl CM, Campagnolo F, Patt M, Schmehl R. Drag power kite with very high lift coefficient. *Renew Energy*. 2017;118:290-305. https://doi.org/10.1016/j.renene.2017.10.073

33. Malz EC, Koenemann J, Sieberling S, Gros S. A reference model for airborne wind energy systems for optimization and control. *Renew Energy*. 2019; 140:1004-1011. https://doi.org/10.1016/j.renene.2019.03.111

34. Harham C Response to the federal aviation authority. Makani Power. Available at http://www.energykitesystems.net/FAA/FAAfromMakani.pdf, Tech. Rep., 2012, (Accessed on: June 17, 2020).

35. Makani Power. Available at. https://makanipower.com (Accessed on June 10, 2020)

36. Roque LAC, Paivab LT, Fernandesb MCRM, Fontesc DBMM, Fontesb FACC. Layout optimization of an airborne wind energy farm for maximum power generation. *Energy Rep*. 2020;6:165-171. https://doi.org/10.1016/j.egyr.2019.08.037

37. Fagiano L Control of tethered airfoils for high-altitude wind energy generation—advanced control methods as key technologies for a breakthrough in renewable energy generation. Ph.D. dissertation, Politecnico di Milano, Available at http://hdl.handle.net/11311/1006424, 2009.

38. GAMS Development Corporation. General Algebraic Modeling System (GAMS Release 27.1.0), Fairfax, VA, USA, 2019.

39. Göransson L, Goop J, Odenberger M, Johnsson F. Impact of thermal plant cycling on the cost-optimal composition of a regional electricity generation system. *Appl Energy*. 2017;197:230-240. https://doi.org/10.1016/j.apenergy.2017.04.018

40. Nilsson K, Unger T Bedömning av en europeisk vindkraftpotential med GIS-analys, 2014. Available on demand.

41. European Commission. NATURA 2000. Available at https://ec.europa.eu/environment/nature/natura2000/, (Accessed on February 10, 2021).

42. Norwood Z, Nyholm E, Otanicar T, Johnsson F. A geospatial comparison of distributed solar heat and power in Europe and the US. *PLoS ONE*. 2014;9(12): 1-31. https://doi.org/10.1371/journal.pone.0112442

43. Rienecker MM, Suarez MJ, Gelaro R, et al. Merra: Nasas modern-era retrospective analysis for research and applications. *J Climate*. 2011;24(14): 3624-3648. https://doi.org/10.1175/JCLI-D-11-00015.1

44. Energi S, Verksamheten E 2015 Available at https://www.energiforetagen.se/globalassets/energiforetagen/statistik/e laret2015_160429_web2.pdf? v=nonce-1845d67a-ef18-4d2e-a741-ce87ba0dbf8e, April 2016, (Accessed on: February 10, 2021).

45. International Energy Agency. World energy outlook. Available at https://www.iea.org/topics/world-energy-outlook, (Accessed on February 10, 2021).

46. Thunman H, Larsson A, Hedenskog M. Commissioning of the GoBiGas 20 MW biomethane plant. The international conference on thermo-chemical conversion science, 2015, Available at: https://research.chalmers.se/publication/509030 (Accessed on: February 10, 2021).

47. Danish Energy Agency. Technology data. Available at: https://ens.dk/en/our-services/projections-and-models/technology-data, May 2018, (Accessed on: July 10, 2020).

48. Taljegard M, Göransson L, Odenberger M, Johnsson F. Impacts of electric vehicles on the electricity generation portfolio—a scandinavian-german case study. *Appl Energy*. 2019;235:1637-1650. https://doi.org/10.1016/j.apenergy.2018.10.133

49. entsoe. Available at https://www.entsoe.eu. (Accessed on February 09, 2021).

50. Loyd ML. Crosswind kite power. *J Energy*. 1980;4:106-111. https://doi.org/10.2514/3.48021

APPENDIX A: TURBINE FUNCTION

The c_p-value is defined by

$$
c_p = \begin{cases} (v_w - v_{cp,maxb})c_{p,slope} + c_{p,maxb} & \text{for } v_{cp,maxb} \leq v_w \leq v_{cp,minb} \\ c_{p,max} & \text{for } v_w \leq v_{cp,maxb} \\ c_{p,min} & \text{for } v_w \geq v_{cp,minb} \end{cases}. \tag{A1}
$$

The rated wind speed is defined by

$$
v_{rat} = \left(\frac{2P_{cap}}{\frac{\pi}{4}D^2 \rho c_{p,max}} \right)^{\frac{1}{3}}, \tag{B1}
$$

where the minimum and maximum break point wind speeds of the c_p value are $v_{cp,maxb} = (v_{rat} - 2)$ and $v_{cp,minb} = (v_{rat} + 7)$. The slope of the c_p-curve is then computed as

$$
c_{p,slope} = \frac{c_{p,max} - c_{p,min}}{v_{cp,maxb} - v_{cp,minb}}.
$$

The values in Table A1 are taken from a previous study.[22]

TABLE A1 Wind turbine parameters

Parameter	Value	Description	Parameter	Value	Description
η_{ext} [−]	0.94	external losses	$c_{p,max}$ [−]	0.45	max c_p value
η_{int} [−]	0.885	internal losses	$c_{p,min}$ [−]	0.18	min c_p value
D [m]	100	rotor diameter	v_{in} [m/s]	3	cut-in wind speed
P_{cap} [MW]	1.94	WT generator size	v_{out} [m/s]	25	cut-out wind speed

APPENDIX B: ENERGY SYSTEM MODEL

B.1 | Mathematical model of electricity system

The electricity system is formulated as a linear programming (LP) problem with the objective of minimizing the total annual system costs. The included sets (upper-case letters in curly font), parameters (upper-case letters), and variables (lower-case letters) are listed in Table B1. The technology data relevant for this study are listed in Table B2.

The LP problem is formulated in Section 2.3 by the problem objective (4), the load-supply balance equations (5), the capacity limits (6), the constrained area for wind technology installations (7), and the fixed electricity share that is supplied by AWESs (8). Further constraints are included concerning hydro power, thermal generation and emissions.

Hydro power

The current storage of hydro power $soc_{hydro,t}$ at time t is constrained by the water reservoir, the maximum power plant capacity, and the weather-dependent inflow q_t^{in} as

$$soc_{hydro,t} \leq s_{hydro} \quad \forall t \in \mathcal{T}$$
$$soc_{hydro,t+1} \leq soc_{hydro,t} + q_t^{in} - g_{hydro,t} \quad \forall t \in \mathcal{T}$$

Thermal cycling

Thermal power production technologies are limited by their cycling (start-up and minimal load abilities). The generation of technology i is bounded by the minimum load and the hot capacity, which is defined as

TABLE B1 Sets and variables of the LP problem

Set		Description
$\mathcal{I}$		Set of technologies
$\mathcal{T}$		Set of time steps
$\mathcal{T}_{vRES}$		Subset including all wind power technologies and solar PV
$\mathcal{T}_{th}$		Subset including all thermal technologies
$\mathcal{J}$		Set of time steps comprised in a start-up interval

Variable	Unit	
$g_{i,t}$	GW	Generation of technology i at time step t
s_i	GW	Installed capacity of technology i
$g_{i,t}^{active}$	GW	Active capacity of a technology i at a time t
$c_{i,t}^{cycl}$	k€	Cycling cost
$c_{i,t}^{start}$	k€	Start-up cost
$c_{i,t}^{part-load}$	k€	Part-load cost

Parameter	Unit	Description
D_t	GWh	Electricity demand of a region at time step t
L_i^{min}		Minimum relative load level for a technology i
ρ_P	$^{MW}/_{km^2}$	Power density for either AWE or WT
A_k	km^2	Area available for wind installment in class k
$G_{i,t}$	-	Weather-dependent profile for technology i at time t
C_i^{inv}	k€	Investment cost of technology i
C_i^{run}	k€	Running cost of technology i

TABLE B2 Costs of the technologies and fuels used in the electricity system analysis

Technology	capital cost [€/kW]	var.O&M [€/MWh]	fix.O&M [€/kWyear]	min. load [−]	life time [year]	start time [h]
WT	1290	1.1	12.60	-	30	0
Solar PV	418	1.1	6.50	-	40	0
Hydro	2468	1.0	56.62	-	500	0
Biogas CCT [a]	932	0.8	12.96	0.3	30	6
Biogas GT [b]	466	0.7	7.92	0.3	30	0
Bio-NG CCS [c]	1626	2.1	40.25	0.3	30	12
Nuclear	4124	0	153.7	0.7	60	24
AWE [d]	-	-	-	-	30	0

[a]CCT: Combined cycle gas turbine.
[b]GT: Open cycle gas turbine.
[c]CCS: Carbon capture and storage.
[d]AWE Airborne wind energy: costs are varied in the modelling.

$$g_{i,t} \leq g_{i,t}^{\text{active}} \quad \forall t \in \mathcal{T}, i \in \mathcal{I}_{\text{th}},$$

where $\mathcal{I}_{\text{th}}$ is the set of thermal power plants and g^{active} is the active capacity of a technology i at each time step t. If a plant i is active, the active generation needs to be larger than the minimum load level L_i^{min} as

$$L_i^{\text{min}} g_{i,t}^{\text{active}} \leq g_{i,t} \quad \forall t \in \mathcal{T}, i \in \mathcal{I}_{\text{th}} \text{ and } L_i^{\text{min}} = [0,1]$$

The start-up capacity $g_{i,t}^{\text{start}}$ at time t of a technology i is constrained by the current active capacity as

$$g_{i,t}^{\text{start}} \geq g_{i,t}^{\text{active}} - g_{i,t-1}^{\text{active}} \quad \forall t \in \mathcal{T}, i \in \mathcal{I}_{\text{th}}$$

and constrained by the minimum start-up time as

$$g_{i,t}^{\text{start}} \leq s_i - g_{i,t-j}^{\text{active}} \quad \forall t \in \mathcal{T}, j \in \mathcal{J}, i \in \mathcal{I}_{\text{th}},$$

where $\mathcal{J}$ is a set of time steps comprised in the start-up interval.

The related cycling costs are then a combination of start-up c_i^{start} and part-load costs $c_i^{\text{part-load}}$ and defined as

$$c_{i,t}^{\text{cycl}} \geq g_{i,t}^{\text{start}} C_i^{\text{start}} + (g_{i,t}^{\text{active}} - g_{i,t}) C_{i,t}^{\text{part-load}} \quad \forall t, \in \mathcal{T}, i \in \mathcal{I}_{\text{th}}$$

Emissions

The total electric power production is constrained by the annual net emissions as

$$\sum_{t \in \mathcal{T}} \sum_{i \in \mathcal{I}_{\text{th}}} E_i g_{i,t} \frac{1}{\eta_i} + E^{\text{start}} g_{i,t}^{\text{start}} + E_i^{\text{part}} (g_{i,t}^{\text{active}} - g_{i,t}) \leq E_{\text{cap}},$$

where E_{cap} is the total allowed emission in kg of the system in one year. In this study $E_{\text{cap}} = 0$.